Report

Current Biology

Area Prostriata in the Human Brain

Highlights

- We describe here the functional properties of visual cortical area prostriata
- It has a complete and orderly representation of the contralateral visual field
- Receptive fields are large and equally distributed across the visual field
- The area shows a clear preference for very fast motion, up to 500°/s

Authors

Kyriaki Mikellidou, Jan W. Kurzawski, Francesca Frijia, Domenico Montanaro, Vincenzo Greco, David C. Burr, Maria Concetta Morrone

Correspondence

kmikellidou@gmail.com

In Brief

Mikellidou et al. describe functionally area prostriata in humans. Located at the fundus of the calcarine sulcus, it has an orderly representation of the contralateral visual field, evenly distributed receptive fields, and a preference for fast motion. Prostriata may be alerting the brain to rapidly appearing visual events, mainly in the periphery.

Mikellidou et al., 2017, Current Biology *27*, 1–5
October 9, 2017
http://dx.doi.org/10.1016/j.cub.2017.08.065

CellPress

Please cite this article in press as: Mikellidou et al., Area Prostriata in the Human Brain, Current Biology (2017), http://dx.doi.org/10.1016/j.cub.2017.08.065

Current Biology
Report

Area Prostriata in the Human Brain

Kyriaki Mikellidou,[1,7,*] Jan W. Kurzawski,[2,3] Francesca Frijia,[4] Domenico Montanaro,[4] Vincenzo Greco,[5] David C. Burr,[3,6] and Maria Concetta Morrone[1,2]
[1]Department of Translational Research on New Technologies in Medicine and Surgery, University of Pisa, via Savi 10, 56126 Pisa, Italy
[2]Stella Maris Scientific Institute, Viale del Tirreno, 331, 56128 Calambrone, Italy
[3]Department of Neuroscience, Psychology, Pharmacology and Child Health, University of Florence, Via di San Salvi 12, 50139 Florence, Italy
[4]Unit of Neuroradiology, Fondazione CNR/Regione Toscana G. Monasterio, Via Giuseppe Moruzzi 1, 56124 Pisa, Italy
[5]Istituto Nazionale di Ottica, CNR, Largo Enrico Fermi 6, 50125 Florence, Italy
[6]Neuroscience Institute, CNR, Via Giuseppe Moruzzi 1, 56124 Pisa, Italy
[7]Lead Contact
*Correspondence: kmikellidou@gmail.com
http://dx.doi.org/10.1016/j.cub.2017.08.065

SUMMARY

Area prostriata is a cortical area at the fundus of the calcarine sulcus, described anatomically in humans [1–5] and other primates [6–9]. It is lightly myelinated and lacks the clearly defined six-layer structure evident throughout the cerebral cortex, with a thinner layer 4 and thicker layer 2 [10], characteristic of limbic cortex [11]. In the marmoset and rhesus monkey, area prostriata has cortical connections with MT+ [12], the cingulate motor cortex [8], the auditory cortex [13], the orbitofrontal cortex, and the frontal polar cortices [14]. Here we use functional magnetic resonance together with a wide-field projection system to study its functional properties in humans. With population receptive field mapping [15], we show that area prostriata has a complete representation of the visual field, clearly distinct from the adjacent area V1. As in the marmoset, the caudal-dorsal border of human prostriata—abutting V1—represents the far peripheral visual field, with eccentricities decreasing toward its rostral boundary. Area prostriata responds strongly to very fast motion, greater than 500°/s. The functional properties of area prostriata suggest that it may serve to alert the brain quickly to fast visual events, particularly in the peripheral visual field.

RESULTS

Prostriata is difficult to study functionally, as it lies adjacent to the far periphery representation of primary visual cortex (V1), in the fundus of the calcarine sulcus. We therefore used a powerful model-driven approach—population receptive field (pRF) mapping—to compute visual field maps [15] over a wide range of eccentricities, up to ~60° (see STAR Methods and Figure S1). Figures 1A and 1B show left hemisphere meshes with overlaid pRF eccentricity and polar maps of the occipital pole for four example subjects (other subjects in Figure S2A). The dashed lines show the borders between V1, V2, and V3. Moving anteriorly in the eccentricity maps from the occipital pole (the foveal representation of V1) toward the parieto-occipital sulcus (POS), following the representation of the horizontal meridians of the polar maps in V1 (red color code of Figure 1B), there is a clear progression in the representation of eccentricity, up to ~60° (purple color code in Figure 1A). Larger eccentricities should be represented in less than 2 mm (calculated based on [16]). At the intersection of the calcarine sulcus and the POS, the eccentricity representation begins to decrease, consistently across subjects. In the cortical space around this inversion, between the mapping of 60° in the calcarine sulcus and the most central visual field representation in the POS, there appears to be a complete independent map of the contralateral visual field (dashed white outlines of the meshes of Figures 1A, 1B, and S2A). Given the position of this map, it likely represents prostriata in humans.

Figure 2A plots the variation in eccentricity along a line in cortical space connecting the foveal representation in V1 to that in the POS, passing through the point of the highest eccentricity in the calcarine sulcus for each individual participant (which we define as origin). Eccentricity first increases throughout V1, then rapidly decreases within a space of 10–20 mm (mean = 14.5 mm, SD = 3.5 mm) through the most anterior portion. The goodness of fit of the model (heatmap in Figure 2A) was significant across participants along the entire calcarine sulcus, through V1 and into the POS region ($p < 0.005$). Figure 2B summarizes the polar representations of all subjects. The upper and lower visual fields (yellow and green, respectively) were represented in similar proportions, but there was a stronger horizontal than vertical representation, which may result from the more extensive horizontal than vertical stimulation (60° cf. 42°). A similar asymmetry was observed in V1 (see Figure S2D).

Figure S2B shows that the receptive field coverage of the putative prostriata (the region around the intersection of calcarine and POS) is quite uniform, with no tendency of magnification of central vision. V1, on the other hand, has more voxels dedicated to central vision, following the well-known magnification seen in many visual areas [17, 18] (Figure S2C). Although our stimuli were not optimized to measure receptive field (RF) size in the far periphery, the maps of Figure S2E show that moving anteriorly along the calcarine sulcus, there is a clear increase in RF size, remaining large over all prostriata except the foveal representation in the POS. All these facts combine to suggest the existence of a complete contralateral visual field representation

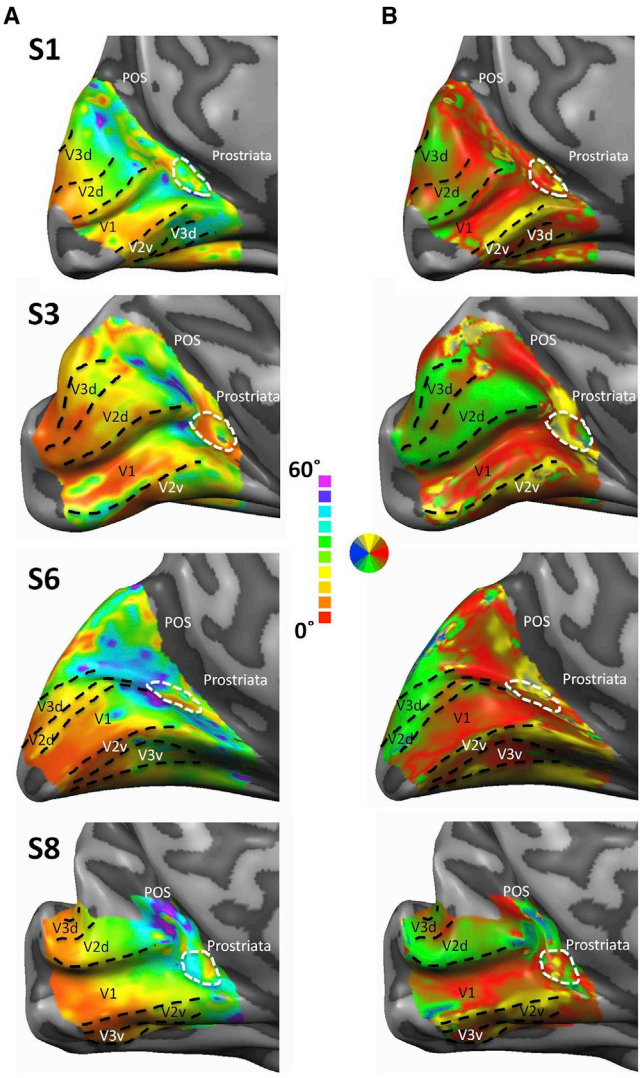

Figure 1. Visual Field Maps Showing Eccentricity and Polar Angle Representations throughout the Medial Occipital Lobe

(A) Semi-inflated meshes of the left hemisphere for four representative subjects, showing eccentricity representation throughout the medial part of the occipital lobe.

(B) Polar angle representations in the same region. Dashed black lines show the borders between V1, V2, and V3; dotted white lines enclose the putative functional region associated with prostriata.

See also Figure S1.

inside a region corresponding to that described in the marmoset monkey [7] and defined anatomically in human [5] as prostriata. The Talairach coordinates of the average barycenter (n = 9) of this area is X: −19.8 ± 1.7, Y: −60.7 ± 3.0, Z: 1.4 ± 4.5, very similar to that which can be calculated from the average of Glasser and colleagues' [5] 210 subjects: X: −22.0, Y: −55.7, Z: 2.5.

We have previously compared blood-oxygen-level-dependent (BOLD) responses to moderate-speed (38°/s) and very fast (570°/s) motion and reported similarly strong and significant responses to both speeds in both central and in peripheral visual fields in the majority of visual areas along the dorsal and ventral visual pathways (K.M., F.F., D.M., V.G., D.C.B., and M.C.M., unpublished data). However, in only one area, close to what we describe here as prostriata, did we observe a preferential response to very fast motion. We confirm this preference in the current study. Figure 3A shows the contrast between moderate and very fast gratings on the posterior pole of the semi-inflated mesh surfaces of the left hemispheres of three representative participants (S3, S8, S9; blue and green indicate preference for fast speed; red and yellow indicate moderate speed). The distinct preference for fast motion is evident at the fundus of the calcarine sulcus and beyond, extending into the POS and into area prostriata (as defined by our pRF techniques). Figure 3B shows for each observer the modulation of BOLD response of area prostriata to very fast and moderate speeds, compared with homogeneous fields. For all subjects, the response was far stronger to fast than to moderate-speed gratings (0.55 ± 0.22 compared with −0.02 ± 0.22; $t(8) = 7.05$, $p < 0.0001$).This is the first example of a clear-cut functional preference for very fast motion in any human visual area. Interestingly, it is similar to area prostriata in the marmoset monkey [7]. The pattern of results for V1 was quite different (Figure 3C), with the average responses to the two types of motion stimuli very similar (fast: 0.52 ± 0.43; moderate: 0.51 ± 0.33; $t(8) = 0.06$, $p = 0.95$).

We also recorded a weaker response in a region corresponding to prostriata in the right hemisphere (Figure S3A). This right hemisphere region also preferred very fast motion (Figure S3B). The weaker BOLD response probably results from our stimuli extending only 25° into the left visual field, suggesting that area prostriata requires large stimuli to evoke strong BOLD responses, consistent with its uniform representation of the visual field up to 40° of visual eccentricity (Figure S2B).

To confirm that the visual response was selective to the direction of motion (rather than a spurious response to flicker), in four subjects we measured the BOLD response separately to left- and right-drifting gratings and decoded the two directions of motion with a multi-voxel pattern analysis (MVPA) technique. The stars of Figure 3D indicate that support vector machine (SVM) classification accuracy was significantly above chance for all four subjects, assessed by bootstrap sign test, for both prostriata and V1.

DISCUSSION

We have examined the functional specificity of area prostriata in the human brain, previously described by anatomical means [1–5]. This cortical area responds preferentially to rapid motion over a wide visual field, extending up to ~60° into the far periphery, and has clear selectivity for very fast motion. The functional characteristics of area prostriata point to an active role in processing visual information from the periphery, with more voxels dedicated to the peripheral than the central visual field. The homogeneous coverage of the visual field and preference for fast speeds may explain why other researchers have not described this area functionally, as standard stimulation techniques typically extend no further than 10°, with speeds less than 30°/s. However, there are hints in the literature of functional responses to prostriata in humans. For example, the pRF maps of Mackey et al. [19] show clear activation in two subjects along the calcarine sulcus, responding to stimuli of

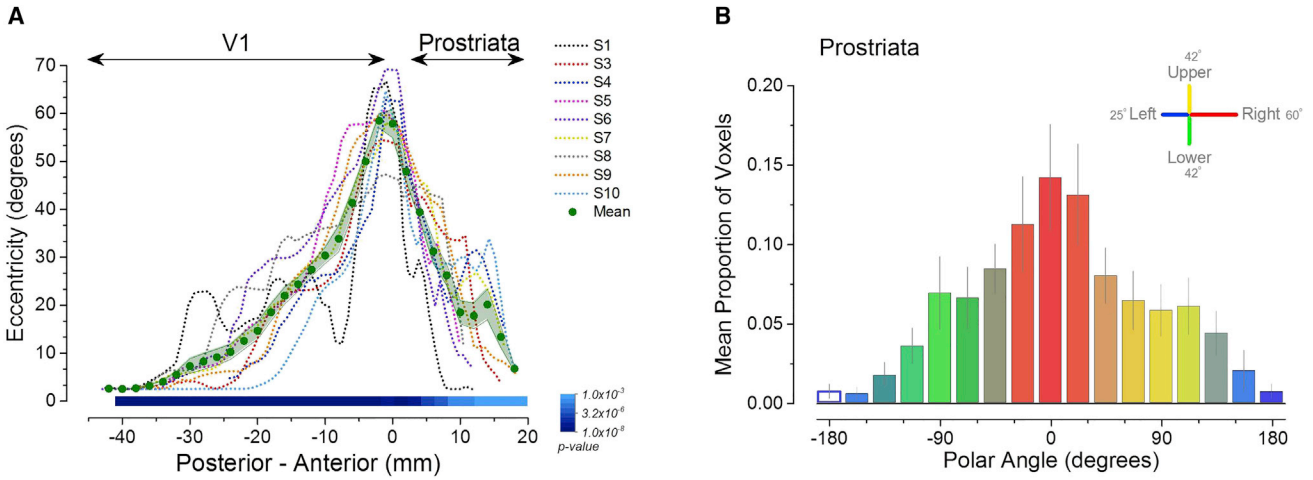

Figure 2. pRF Mapping Reveals a Foveal Representation at the Anterior End of the Calcarine Sulcus, Consistent with Area Prostriata, which Has a Full Representation of the Contralateral Visual Field

(A) Eccentricity representation along the calcarine sulcus, for each subject (color code at right), with large green dots and shading showing the mean and ±1 SEM. Along this axis (described in text), there are two representations of central vision, at around −40 mm and +20 mm, of V1 and prostriata, respectively. The lower heatmap shows the average significance of the correlation of the pRF model fit (n = 9).

(B) Histogram showing the proportion of voxels (averaged over participants) responding to each polar angle within area prostriata (n = 9). Error bars show ±1 SEM. See also Figure S2.

12° eccentricity, distinct from V1 and consistent with the position of prostriata (their Figure S2). An earlier report using extended peripheral stimulation also shows an inversion of polar angle sign at a location consistent with area prostriata (their Figures 1 and 2) [20].

Although our methods lack the fine-grain resolution to map precisely the representations of polar angles within prostriata, they suggest an inversion of sign of upper and lower fields. In most of our subjects, the lower visual field is consistently represented more ventrally than the upper visual field, similar to that reported for area V6 [20, 21]. The polar maps are not completely orthogonal to the eccentricity maps in all subjects, unlike most reports of V1, V2, and V3. However, the gradients are not perfectly parallel either, allowing the area to represent the entire contralateral hemifield. This is similar to reported maps of intraparietal and frontal cortex [19] and also of the lateral occipital complex [22]. Higher-order areas tend to have large RFs, best mapped with large stimuli, making it difficult for linear RF models to accurately characterize angle and eccentricity. This problem is exacerbated in the far periphery.

Moving dorsally along the POS from prostriata to V6, another small area has been segmented on anatomical criteria [5]. It is possible that this area may show the same rule of inversion of visual field map as described here for prostriata. However, if such a visual area does exist, it did not respond well to our battery of stimuli and to very fast motion; further dedicated experiments would be needed to explore its possible functional specialization.

Previous anatomical studies have shown that area prostriata in primates is connected with multiple and diverse cortical areas, including visual [12], auditory [13, 23], and motor [8] areas as well as association areas in the cingulate [24], parahippocampal [25], posterior parietal [23], and various frontal [14] regions. In non-human primates, prostriata neurons have large RFs (~30°), extending into the far periphery [7]. Their physiological properties are similar to early sub-cortical structures, such as the lateral geniculate nucleus and the superior colliculus: they have high spontaneous activity, robustly short latencies to visual stimulation, and preference for high speeds but little other stimulus selectivity and weak adaptation to repeated stimulation [7]. Such a cortical network could act to monitor the peripheral visual field for new and unexpected stimuli to shift attention rapidly and generate coordinated defensive responses. This would be consistent with the response to fast motion, and the strong representation of the peripheral field, reported here for humans and observed in other primates [7]. The known connections of area prostriata with motor areas controlling the head and upper limb musculature [8] as well as the importance of the peripheral visual field (via the monocular crescents) in head and body stabilization [26] would be consistent with this idea. Perhaps the specialization of prostriata within these general goals is the rapid processing of peripheral signals.

Why the preference for such fast motion? Under natural conditions, fast motion occurs under two general conditions: when we make saccadic eye movements (300–600°/s) and when objects move very close to us (or we move close to stationary objects). In the case of eye movements, we are typically unaware of the fast image motion saccades generate, presumably because motion areas stimulated during saccades are to some extent suppressed [27, 28]. Area prostriata could be one of the areas involved with the suppression. On the other hand, fast motion near the eye, not generated by the motion of the eye itself, could be a potential danger, requiring urgent action. And fast peripheral image motion caused by our motion through the environment may be essential for navigation. The anatomical proximity of area prostriata to the retrosplenial cortex, which has been implicated in spatial navigation is consistent with this notion [29].

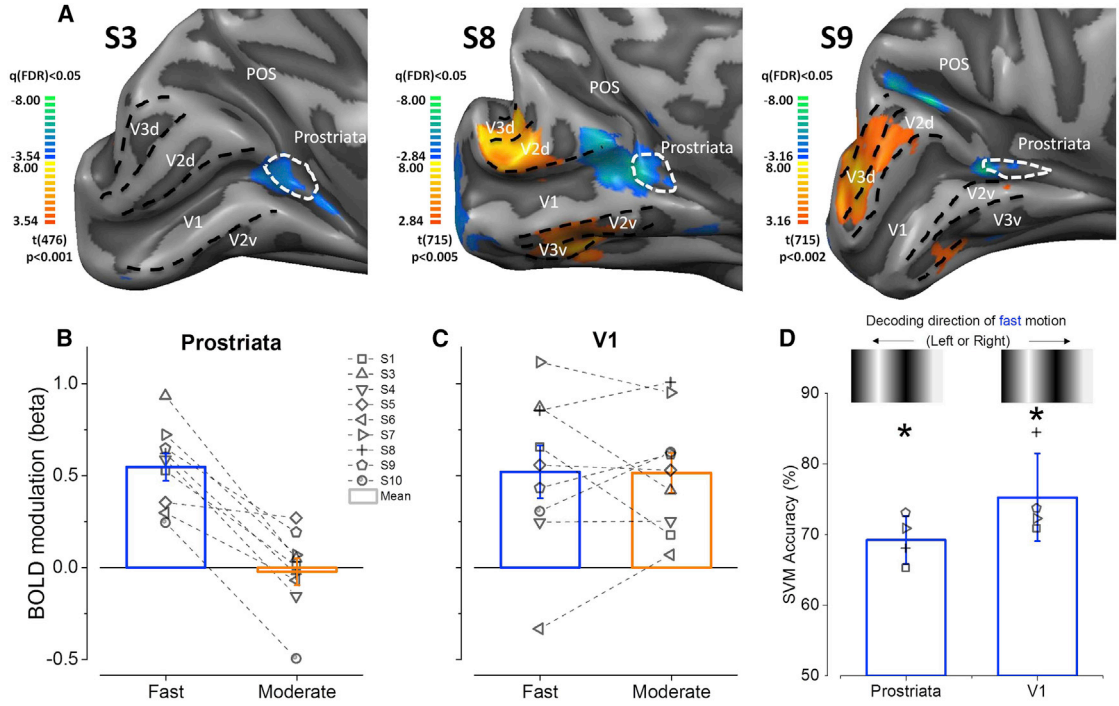

Figure 3. BOLD Response to Moving Gratings

(A) Contrast maps on semi-inflated meshes of the hemisphere showing preferential activation to fast (blue) and moderate-speed (orange) gratings for three representative participants (S3, S8, and S9). Black dotted lines indicate the boundaries between area V1, V2, and V3. Area prostriata is encircled in a dotted white contour.

(B) BOLD modulation of area prostriata to stimulation by fast and moderate-speed motion for nine observers. The bars show the mean response (blue to fast, orange to moderate speeds); symbols show the response of individual observers. A similar pattern of responses was observed in the right hemisphere, where the stimulated visual field was ~25° (see Figure S3B). Error bars show ±1 SEM.

(C) BOLD modulation of area V1 to stimulation by fast and moderate-speed motion for nine observers. Conventions are the same as they are in (B). Error bars show ±1 SEM.

(D) Average classification accuracy of a linear SVM for direction of fast motion in area prostriata and V1 (n = 4). The dotted horizontal line indicates performance at chance level (50%). Error bars show SD of classification accuracy. To yield an estimate of significance, we used a bootstrap sign test. Performance of the SVM in all four subjects was significantly above chance level both for area prostriata (mean S1 = 65.2, S7 = 70.8, S8 = 68, S9 = 73; p = 0.03) and V1 (mean S1 = 70.8, S7 = 72.2, S8 = 84.4, S9 = 73.7; p = 0.01).

To conclude, while central vision is essential for analysis of fine detail, the peripheral visual field is responsible for shifts of attention and initiation of quick action when required through a complex network of diverse cortical areas. The unique functionality and structural connectivity of area prostriata suggests the existence of a specialized cortical area for peripheral visual field processing, disseminating information to multiple cortical areas.

STAR★METHODS

Detailed methods are provided in the online version of this paper and include the following:

- KEY RESOURCES TABLE
- CONTACT FOR REAGENT AND RESOURCE SHARING
- EXPERIMENTAL MODEL AND SUBJECT DETAILS
  - Subject Details
- METHOD DETAILS
  - fMRI scanning
  - Presentation of Visual Stimuli
  - Drifting-Gratings
  - Attentional Task at Central Fixation
  - pRF Mapping Stimuli
- QUANTIFICATION AND STATISTICAL ANALYSIS
  - Data Analysis
  - Estimation of pRF Maps
  - Evaluation of fMRI Activity in Prostriata
  - Support Vector Machine Analysis

SUPPLEMENTAL INFORMATION

Supplemental Information includes three figures and can be found with this article online at http://dx.doi.org/10.1016/j.cub.2017.08.065.

AUTHOR CONTRIBUTIONS

K.M., D.C.B., and M.C.M. designed the experiments. V.G. designed and built the custom-made magnetic-imaging-compatible visual projection system. K.M., F.F., D.M., and M.C.M. performed the experiments and K.M. and J.W.K. analyzed the results. K.M., J.W.K., D.C.B., and M.C.M. wrote the manuscript. All authors revised the manuscript. D.C.B. and M.C.M. supervised the project.

ACKNOWLEDGMENTS

This research was supported by the European Research Council under the European Union's Seventh Framework Programme (FPT/2007-2013) under grant agreement number 338866 (K.M., D.C.B., and M.C.M.) and by the European Union's Horizon 2020 Research and Innovation Programme under the Marie Sklodowska-Curie grant agreement number 641805 (J.W.K.). We would like to thank Niccolò Calcini for help with cortex segmentations, Guido Marco Cicchini for help with stimuli setup, and Paola Binda for invaluable advice on pRF mapping.

Received: March 6, 2017
Revised: May 31, 2017
Accepted: August 25, 2017
Published: September 28, 2017

REFERENCES

1. Sanides, F. (1969). Comparative architectonics of the neocortex of mammals and their evolutionary interpretation. Ann. N Y Acad. Sci. *167*, 404–423.
2. Sanides, F., and Vitzthum, H.G. (1965). Zur Architektonik der menschlichen Sehrinde und den Prinzipien ihrer Entwicklung. Deutsche Zeitschrift für Nervenheilkunde *187*, 680–707.
3. Sanides, F. (1970). Functional architecture of motor and sensory cortices in primates in the light of a new concept of neocortex evolution. In The Primate Brain, C.R. Noback, and W. Montagna, eds. (Appleton-Century-Crofts), pp. 137–208.
4. Ding, S.-L.L., Royall, J.J., Sunkin, S.M., Ng, L., Facer, B.A., Lesnar, P., Guillozet-Bongaarts, A., McMurray, B., Szafer, A., Dolbeare, T.A., et al. (2016). Comprehensive cellular-resolution atlas of the adult human brain. J. Comp. Neurol. *524*, 3127–3481.
5. Glasser, M.F., Coalson, T.S., Robinson, E.C., Hacker, C.D., Harwell, J., Yacoub, E., Ugurbil, K., Andersson, J., Beckmann, C.F., Jenkinson, M., et al. (2016). A multi-modal parcellation of human cerebral cortex. Nature *536*, 171–178.
6. Rosa, M.G.P., Casagrande, V.A., Preuss, T., and Kaas, J.H. (1997). Visual field representation in striate and prestriate cortices of a prosimian primate (Galago garnetti). J. Neurophysiol. *77*, 3193–3217.
7. Yu, H.H., Chaplin, T.A., Davies, A.J., Verma, R., and Rosa, M.G.P. (2012). A specialized area in limbic cortex for fast analysis of peripheral vision. Curr. Biol. *22*, 1351–1357.
8. Morecraft, R.J., Rockland, K.S., and Van Hoesen, G.W. (2000). Localization of area prostriata and its projection to the cingulate motor cortex in the rhesus monkey. Cereb. Cortex *10*, 192–203.
9. Kobayashi, Y., and Amaral, D.G. (2003). Macaque monkey retrosplenial cortex: II. Cortical afferents. J. Comp. Neurol. *466*, 48–79.
10. Ding, S.-L., Morecraft, R.J., and Van Hoesen, G.W. (2003). Topography, cytoarchitecture, and cellular phenotypes of cortical areas that form the cingulo-parahippocampal isthmus and adjoining retrocalcarine areas in the monkey. J. Comp. Neurol. *456*, 184–201.
11. Rockland, K.S. (2012). Visual system: prostriata–a visual area off the beaten path. Curr. Biol. *22*, R571–R573.
12. Palmer, S.M., and Rosa, M.G.P. (2006). A distinct anatomical network of cortical areas for analysis of motion in far peripheral vision. Eur. J. Neurosci. *24*, 2389–2405.
13. Falchier, A., Schroeder, C.E., Hackett, T.A., Lakatos, P., Nascimento-Silva, S., Ulbert, I., Karmos, G., and Smiley, J.F. (2010). Projection from visual areas V2 and prostriata to caudal auditory cortex in the monkey. Cereb. Cortex *20*, 1529–1538.
14. Burman, K.J., Reser, D.H., Yu, H.H., and Rosa, M.G.P. (2011). Cortical input to the frontal pole of the marmoset monkey. Cereb. Cortex *21*, 1712–1737.
15. Dumoulin, S.O., and Wandell, B.A. (2008). Population receptive field estimates in human visual cortex. Neuroimage *39*, 647–660.
16. Wu, J., Yan, T., Zhang, Z., Jin, F., and Guo, Q. (2012). Retinotopic mapping of the peripheral visual field to human visual cortex by functional magnetic resonance imaging. Hum. Brain Mapp. *33*, 1727–1740.
17. Engel, S.A., Glover, G.H., and Wandell, B.A. (1997). Retinotopic organization in human visual cortex and the spatial precision of functional MRI. Cereb. Cortex *7*, 181–192.
18. Benson, N.C., Butt, O.H., Datta, R., Radoeva, P.D., Brainard, D.H., and Aguirre, G.K. (2012). The retinotopic organization of striate cortex is well predicted by surface topology. Curr. Biol. *22*, 2081–2085.
19. Mackey, W.E., Winawer, J., and Curtis, C.E. (2017). Visual field map clusters in human frontoparietal cortex. eLife *6*, e22974.
20. Pitzalis, S., Galletti, C., Huang, R.S., Patria, F., Committeri, G., Galati, G., Fattori, P., and Sereno, M.I. (2006). Wide-field retinotopy defines human cortical visual area v6. J. Neurosci. *26*, 7962–7973.
21. Pitzalis, S., Sereno, M.I., Committeri, G., Fattori, P., Galati, G., Patria, F., and Galletti, C. (2010). Human v6: the medial motion area. Cereb. Cortex *20*, 411–424.
22. Larsson, J., and Heeger, D.J. (2006). Two retinotopic visual areas in human lateral occipital cortex. J. Neurosci. *26*, 13128–13142.
23. Rockland, K.S., and Ojima, H. (2003). Multisensory convergence in calcarine visual areas in macaque monkey. Int. J. Psychophysiol. *50*, 19–26.
24. Morecraft, R.J., Cipolloni, P.B., Stilwell-Morecraft, K.S., Gedney, M.T., and Pandya, D.N. (2004). Cytoarchitecture and cortical connections of the posterior cingulate and adjacent somatosensory fields in the rhesus monkey. J. Comp. Neurol. *469*, 37–69.
25. Blatt, G.J., Pandya, D.N., and Rosene, D.L. (2003). Parcellation of cortical afferents to three distinct sectors in the parahippocampal gyrus of the rhesus monkey: an anatomical and neurophysiological study. J. Comp. Neurol. *466*, 161–179.
26. Bessou, M., Séverac Cauquil, A., Dupui, P., Montoya, R., and Bessou, P. (1999). Specificity of the monocular crescents of the visual field in postural control. C. R. Acad. Sci. III *322*, 749–757.
27. Ross, J., Morrone, M.C., Goldberg, M.E., and Burr, D.C. (2001). Changes in visual perception at the time of saccades. Trends Neurosci. *24*, 113–121.
28. Morrone, M.C. (2014). Interaction between eye movements and vision: perception during saccades. In The New Visual Neurosciences, 2nd Edition, J.S. Werner, and L.M. Chalupa, eds. (MIT Press), pp. 947–962.
29. Vann, S.D., Aggleton, J.P., and Maguire, E.A. (2009). What does the retrosplenial cortex do? Nat. Rev. Neurosci. *10*, 792–802.
30. Brainard, D.H. (1997). The psychophysics toolbox. Spat. Vis. *10*, 433–436.
31. Kleiner, M., Brainard, D., Pelli, D., Ingling, A., Murray, R., and Broussard, C. (2007). What's new in Psychtoolbox-3. Perception *36*, 1–16.
32. Greco, V., Frijia, F., Mikellidou, K., Montanaro, D., Farini, A., D'Uva, M., Poggi, P., Pucci, M., Sordini, A., Morrone, M.C., et al. (2016). A low-cost and versatile system for projecting wide-field visual stimuli within fMRI scanners. Behav. Res. Methods *48*, 614–620.
33. Sereno, M.I., Dale, A.M., Reppas, J.B., Kwong, K.K., Belliveau, J.W., Brady, T.J., Rosen, B.R., and Tootell, R.B. (1995). Borders of multiple visual areas in humans revealed by functional magnetic resonance imaging. Science *268*, 889–893.
34. Wandell, B.A., Brewer, A.A., and Dougherty, R.F. (2005). Visual field map clusters in human cortex. Philos. Trans. R. Soc. Lond. B Biol. Sci. *360*, 693–707.

STAR★METHODS

KEY RESOURCES TABLE

REAGENT or RESOURCE	SOURCE	IDENTIFIER
Software and Algorithms		
Brain Voyager QX 20.2	BrainInnovation B.V.	SCR_013057
MATLAB 2016b	MathWorks	SCR_001622
Psychtoolbox-3	[30]	SCR_002881

CONTACT FOR REAGENT AND RESOURCE SHARING

Further information and requests for resources should be directed to and will be fulfilled by the Lead Contact, Kyriaki Mikellidou (kmikellidou@gmail.com). There is no restriction for distribution of materials.

EXPERIMENTAL MODEL AND SUBJECT DETAILS

The study was approved by the ethics committee of the Azienda Ospedaliero-Universitaria Pisana (protocol number 3255, approved on 20/01/2009), and was in accordance with the ethical standards of the 1964 Declaration of Helsinki. Informed written consent was obtained from each participant prior to scanning sessions, in accordance with the guidelines of the MRI Laboratory.

Subject Details

Ten healthy participants (25–58 years old, 3 female, all right-handed) with normal or corrected-to-normal visual acuity were scanned. One participant was excluded because of excessive head motion during the scans.

METHOD DETAILS

fMRI scanning

Scanning was performed with a GE 3T scanner (Excite HDx, GE Medical Systems, Milwaukee, WI) at the Fondazione CNR/Regione Toscana G. Monasterio in Pisa, Italy. Each fMRI session comprised six functional and one structural scans.

Three-dimensional (3-D) anatomical images were acquired at 1 × 1 × 1 mm resolution using a T1-weighted magnetization-prepared fast Spoiled Gradient Echo (SPGR) sequence (FOV = 256 mm, BW = 15.63, 256 × 256 matrix, TE = minimum full). Retinotopic maps were acquired with Echo Planar Imaging (EPI) sequencing (FOV = 240 mm, 128 × 128 matrix, slice thickness = 3 mm, 19 axial slices, flip angle = 90°, TE = 30 ms, TR = 2,500 ms). EPI sequencing was also used for acquisition of cortical motion-sensitivity maps (FOV = 240 mm, 128 × 128 matrix, slice thickness = 3 mm, 19 axial slices, flip angle = 90°, TE = 30 ms, TR = 1,500 ms), as well as for acquisition of high-speed drifting grating maps for SVM analysis for four out of ten participants (FOV = 240 mm, 128 × 128 matrix, slice thickness = 2.4 mm, 30 axial slices, flip angle = 90°, TE = 40 ms, TR = 3,000 ms). The first 4–5 volumes of each functional acquisition were discarded from data analysis to achieve a steady state.

Presentation of Visual Stimuli

Drifting gratings and conventional retinotopic mapping stimuli were generated on a VSG 2/5 Visual Stimulus Generator (Cambridge Research Systems) controlled by MATLAB programs (the MathWorks, Natick, MA) in conjunction with routines from the Psychtoolbox [30, 31]. All participants viewed stimuli monocularly through the right eye through a 10–12D correction lens depending on subject refraction, with the left eye obscured by a black patch. Stimuli were projected onto a translucent screen 9 cm from the subject's eye, using a fiber optic system (resolution 10,000 fibers, 60 Hz [32]). The visible screen extended 60° to the right and 25° to the left, and ± 42° vertically.

Drifting-Gratings

We stimulated the visual cortex with large-field (~60°) gratings drifting at moderate and high speeds. The two types of gratings had identical contrast (50%), average luminance (7 cd/m^2) and temporal frequency (10 Hz), differing only in speed and spatial frequency, by a factor of 14. Spatial frequency for high-speed drifting gratings was 0.018 c/° at screen center, corresponding to 571°/s; for moderate-speed drifting gratings spatial frequency was 0.26 c/°, and speed 38°/s. Given that the screen was flat, the spatial frequency (and hence speed) was not constant at the eye, but decreased with eccentricity. However, this distortion was the same for both types of stimuli, and did not influence temporal frequency. We used a block design, with the high-speed and the moderate-speed drifting gratings displayed alternately for a period of 15 s, alternating direction within each block every 2.5 s (starting leftward), each followed by a 15 s blank period. Each block was repeated six times.

For both types of motion stimuli maximum contrast sensitivity was identical in the far periphery compared with full-field stimulation (high-speed gratings ≈230; moderate-speed ≈280; K.M., F.F., D.M., V.G., D.C.B., and M.C.M., unpublished data). At the 50% contrast used during our fMRI session, detection and direction-discrimination of both types of gratings was 100%, both for full-field and peripheral presentation.

For the SVM classification of motion directions, we presented three versions of the high-speed drifting grating: leftward-moving, rightward-moving and stationary. These were presented pseudo-randomly in a block design each lasting 12 s, with each block repeated ten times.

Attentional Task at Central Fixation

During all functional MRI scans with drifting gratings, participants were instructed to maintain central fixation. To assess compliance, and to maintain visual attention during the scan, subjects were required to detect small chromatic variations of the fixation spot throughout the experiment (only possible while fixating), and to keep a mental count of the number of times it was red (on average once every four seconds). Mean accuracy for participants was 98% on this task, suggesting that eye movements were minimal.

pRF Mapping Stimuli

Population RF maps were constructed using (i) horizontal and vertical meridian stimulation, (ii) upper, lower, left and right stimulation of the four visual quadrants, (iii) checkerboard wedge stimuli and (iv) a combination of three sets of checkerboard ring stimuli to map eccentricity.

For (i) we used stimuli comprising 100 circular dots, half black and half white, moving on a gray background in two symmetrical sectors across the fixation point along the two principal meridians [17, 33, 34]. Each dot had a lifetime of 20 frames or 333 ms at a refresh rate of 60 Hz (local speed at linear trajectory = 6.5 degs^{-1}). A block design was used with meridians stimulated interchangeably (6 repetitions) for 15 s and motion direction inverting seven times to avoid BOLD adaptation. For (ii) we used stimuli comprising 250 circular dots, half black and half white, moving on a gray background in four quadrants. Quadrants stimulated sequentially clockwise in a block design, starting from upper right. All other information is identical to (i). For (iii) we divided the visual field into octants of 45 degrees each stimulating sequentially in a single run either the odd or even octants. Each of the four octants within a run appeared on the screen for 15 s, with the last octant followed by a 15 s blank period. This sequence was repeated 6 times.

For (iv), we presented three annuli comprising black and white (∼90% contrast) checks at different eccentricities sequentially for 15 s in a block design starting with the most eccentric stimulus, followed by the medium-sized and foveal stimulus (6 repetitions). The outermost annulus had an outer radius of 60° and an inner radius of 35° of visual angle, confined to the visible screen (extending 60° to the right and 25° to the left, and ± 42° vertically). The medium-sized annulus had an outer radius of 27° and an inner radius of 20° and the central circular stimulus had 8° radius. Two additional runs comprised three rings each (first set 3° − 5.7°, 12.2° − 18.4°, 25° − 35°; second set 0° − 3.5°, 7° − 12.2°, 18.4° − 25°), followed by a blank. Stimuli for these two runs were presented in a pseudo-randomized order, contrast reversal was 4 Hz and contrast was 0.9 over a mean gray background.

QUANTIFICATION AND STATISTICAL ANALYSIS

Data Analysis

Data were analyzed by Brain Voyager QX (Version 20.2, Brain Innovation, Maastricht, Netherlands) and MATLAB (MathWorks, MA). Prior to statistical analysis, functional data underwent standard pre-processing steps including 3-D motion correction, linear trend removal, and high-pass filtering. Slice scan time correction was performed for functional data.

Functional data were co-registered on the 3D anatomical T1-weighted images using a gradient-based affine alignment with the standard Brain Voyager nine parameters (three for translation, three for rotation and three for FOV scale). For each individual participant, anatomical and functional data were transformed first into their own AC-PC space (rotating the cerebrum into the anterior commissure – posterior commissure plane) and then into Talairach space. To generate inflated surfaces for each hemisphere the white–gray boundary was traced, using an automatic segmentation algorithm, supplemented by manual correction by an expert operator to correct errors generated by the automatic routine. This segmentation was also used to automatically reconstruct the surface of the outer gray matter boundary, which was subsequently inflated and flattened.

Estimation of pRF Maps

We used in-built Brainvoyager QX v.20.2 routines for to estimate pRFs using the two-dimensional Gaussian pRF model [15] given by:

$$g(x,y) = e^{-\left(\frac{(x-x_0)^2 + (y-y_0)^2}{2\sigma^2}\right)} \quad \text{(Equation 1)}$$

Where x and y specify the center of the pRFs and σ size. The stimulated and modeled visual field was ± 60 degrees horizontal (x) and ± 42 degrees vertical (y). pRF sizes ranged from 0.2 to 20°, in 30 equal steps. Subsequently, the visual field was divided into a grid of 30 by 30 elements. For each TR, we use the corresponding binarized stimulus frame (stimulated area is white; background is black) irrespective of stimulus carrier and create a binarized version stimulus movie. The number of frames in the movie corresponds to the total number of volumes. A positive response is predicted whenever a stimulus falls on a pRFs and the prediction

is convolved with the hemodynamic response function (HRF). The best model fit for each voxel is obtained by finding values that maximized the correlation between the predicted and actual BOLD response. The eccentricity maps were calculated as:

$$ecc = \sqrt{(x^2 + y^2)} \quad \text{(Equation 2)}$$

Figure S1 of supplemental material shows an example fit for voxels in V1 and prostriata.

Evaluation of fMRI Activity in Prostriata

For each participant, BOLD responses were analyzed using a General Linear Model (GLM) by convolving a box-car function for each stimulation block with a canonical hemodynamic response function (HRF). For each one of these ROIs, an ANOVA was conducted and the beta weights for the two types of motion (fast/moderate) were extracted.

Support Vector Machine Analysis

We use in-built Brainvoyager QX v.20.2 routines to run a linear support vector machine (SVM) classifier with a fixed regularization parameter C = 1 for four participants. For each trial and voxel within the prostriata ROI (as previously defined by pRF mapping) we estimated and z-normalized T values using a two-gamma hemodynamic response function. These values were used for training and testing the linear SVM classifier. The classifier was trained with 70 trials, 35 for each direction of motion, then tested with the 10 left-out trials (5 per direction).For each participant, this procedure was repeated 50 times, with different random draws of the 10 left-out trials. The average accuracy of the classifier across bootstraps was calculated for each participant and is reported as percentage correct.

To test the significance of the decoding accuracy, we ran a permutation bootstrap, where we shuffled the labels of the direction of motion (left- or right-drift) of the training trials, and tested decoding accuracy on the 10 left-out trials. We reiterated this procedure 1,000 times, to perform a sign test of significance (proportion of bootstrapped trials with accuracy greater than with original non-shuffled data).